Int. J. Heat Mass Transfer. Vol. 21, pp. 751–759

0017-9310/78/0601-0751 $02.00/0

HEAT AND MASS TRANSFER IN PACKED BEDS—III. AXIAL MASS DISPERSION

G. LANGER, A. ROETHE, K.-P. ROETHE and D. GELBIN
Central Institute of Physical Chemistry, Academy of Sciences of the GDR, Berlin

(*Received* 28 *March* 1977)

Abstract—Chromatographic techniques and the method of statistical moments are used to determine axial dispersion coefficients of methane in hydrogen on glass balls of different diameters in a laboratory column. Some additional data are available on the axial dispersion of isobutane in air in a bench-scale column with sample withdrawal at varying heights. Dispersion effects may be unpredictable at low column length–diameter ratios. Dispersion coefficients are larger with smaller packing; the limiting value of Pe_∞ at high flowrates increases linearly with packing diameter for $d_p \leqslant 0.25$ cm, and only reaches the generally assumed value of $Pe_\infty = 2$ when $d_p \geqslant 0.3$ cm. These results are explained in terms of a model in which the number of mixing cells in series decreases with particle diameter due to the increasing numbers of particles agglomerated to clusters. Literature correlations for predicting axial dispersion coefficients can lead to good accuracy in technical equipment, but analysis of packed bed processes in a laboratory or bench-scale should include separate investigation of dispersion behavior.

NOMENCLATURE

- D_{AB}, molecular diffusion coefficient [$cm^2 s^{-1}$];
- D_c, pore diffusion coefficient [$cm^2 s^{-1}$];
- D_x, axial diffusion coefficient [$cm^2 s^{-1}$];
- D_{x_E}, eddy diffusion coefficient [$cm^2 s^{-1}$];
- d_p, particle diameter [cm];
- d_R, column diameter [cm];
- K_A, adsorption equilibrium constant;
- k_g, mass-transfer coefficient [$cm\,s^{-1}$];
- m, geometric factor;
- n_a, number of particle layers in axial direction;
- n_r, number of particles in radial direction;
- Pe, Peclet number;
- Pe_∞, Peclet number at infinite velocity;
- R, particle radius [cm];
- Re, Reynolds number;
- t_0, time of flushing the inlet value [s];
- t_d, dead space time [s];
- $\dot{V}$, volume rate of flow [$cm^3 s^{-1}$];
- w, interstitial velocity of flow [$cm\,s^{-1}$];
- x, column length [cm].

Greek symbols

- β, radial dispersion factor;
- β_a, porosity of particle;
- γ, Taylor dispersion constant;
- ε, void fraction of bed;
- μ'_1, 1st absolute moment [s];
- μ_2, 2nd central moment [s^2];
- σ^2, relative standard deviation [%];
- τ, reciprocal axial tortuosity.

INTRODUCTION

IN PART 1 of this series [1] we reviewed the literature and derived the basic equations for determining mass- and heat-transfer coefficients as well as dispersion effects in packed columns with gas or liquid flow. In Part 2 [2] we showed that in small-scale equipment such as is used for experimental purposes, heat-transfer rates are altered appreciably by axial conductivity in the reactor wall. Below we report results on axial dispersion involved in mass-transfer experiments. The axial dispersion coefficient may be correlated to other system parameters by the equation

$$D_x = \tau D_{AB} + \frac{Pe_\infty^{-1} w d_p}{1 + \dfrac{\beta \tau D_{AB}}{w d_p}}. \tag{39}$$

This is identical to equation (8) in part 1, except that there the constants Pe_∞, β were assigned particular values common in the literature, whereas in equation (39) they are considered general parameters. The derivation and physical meaning of equation (39) have been discussed at length by Bischoff [3] and Wicke [4], and will not be treated in detail here. We note that τ is a reciprocal axial tortuosity factor representing the ratio of the distance between two cross sections of a column to the true distance travelled by flowing molecules due to their zig-zag motion between solid particles. Wicke has proposed relating τ to the column void fraction ε,

$$\tau = 0.45 + 0.55\varepsilon. \tag{40}$$

The term $\beta \tau D_{AB}$ accounts for the effects of radial dispersion on the concentration gradients caused by axial dispersion. Using a highly turbulent random walk model, the theoretical value of β is 8.

Bischoff sets

$$Pe_\infty^{-1} = \beta/\gamma \tag{41}$$

where γ is determined by integrating velocity distribution data. In average packed columns Bischoff finds $Pe_\infty^{-1} = 0.45$.

We assume that at high flowrates flow segregation is caused by clusters of solid particles in the column

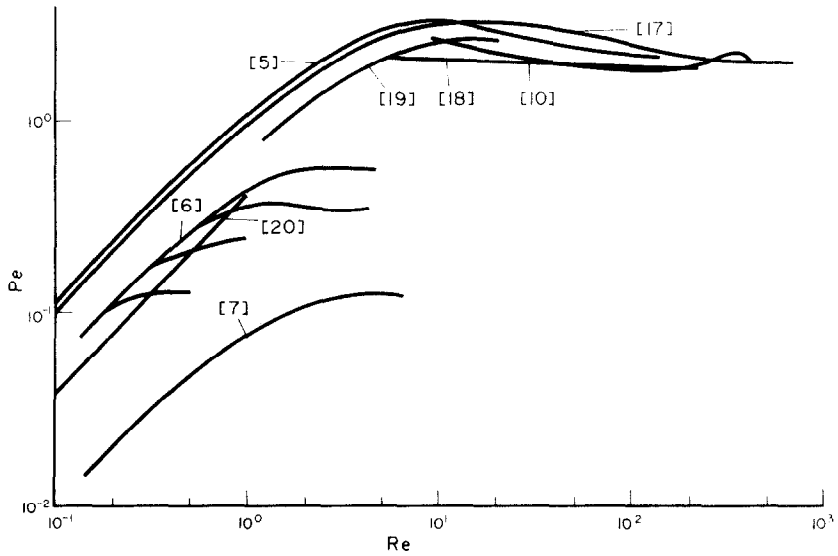

FIG. 1. Literature correlations of Pe vs Re.

having a length equal to $n_a d_p$ and a width equal to $n_r d_p$. Elements of flowing fluid are radially displaced between the lower end of the cluster and the upper end, but mixed in void spaces or cells between adjoining clusters. The overall effect is described by an eddy diffusion coefficient D_{x_L}.

Invoking Einstein's law,

$$D_{x_L} = \frac{(n_a d_p)^2}{2(n_a d_p/w)} = \frac{n_a w d_p}{2} \tag{42}$$

with

$$Pe_r = \frac{w d_p}{D_{x_L}} = \frac{2}{n_a}. \tag{43}$$

This is basically Wicke's model, except that he assumed ideal flow and packing distribution, so that $n_a = 1$. Wicke predicted on this basis $Pe_r^{-1} = 0.5$, in good agreement with Bischoff. We have entered n_a into equation (43) to account for deviations from the ideal model. On the basis of Bischoff's and Wicke's work we can apply the same line of reasoning to the radial dispersion factor, obtaining

$$\beta = \frac{8}{n_r}. \tag{44}$$

Equation (39) may be divided into three regions. At low flowrates, $\beta\tau D_{AB} \gg w d_p$, radial dispersion equalises the effects of flow on axial dispersion, the molecular diffusion term τD_{AB} dominates and the axial dispersion coefficient is independent of velocity. At high flowrates, $\beta\tau D_{AB} < w d_p$, "eddy" or turbulent dispersion dominates and the axial dispersion coefficient increases directly proportional to flowrate. In the intermediate region, $\beta\tau D_{AB} \approx w d_p$, all mechanisms are of importance.

Measuring axial dispersion usually involves the chromatographic method evaluated by means of statistical moments, for example as we have shown in Part 1. A large number of authors have carried out such experiments, with results shown in Fig. 1, where the Peclet number is plotted as a function of the Reynolds number. There is some tendency for results of other authors to fall close to those of Edwards and Richardson [5], but there are noticeable exceptions, particularly the measurements of Suzuki and Smith [6] and Urban and Gomezplata [7]. In Table 1 we list the empiric constants gained by fitting equation (39) to the experimental results of the various authors. In some cases, where basic data had been published, we derived

Table 1. Experimental constants of axial dispersion equation

	x/d_R	d_p [cm]	ε	β	Pe_r
McHenry–Wilhelm [10]	18	0.323			1.88
Edwards–Richardson [5]	10	0.0377–0.607	0.73	13	2.0
Evans–Kenney [11]	164	0.196	0.67*	10*	2.0
Urban–Gomezplata [7]	16	0.6; 1.6	0.73	19	2.0
	16	0.15	0.73	10*	1.0*
Scott–Lee–Papa [12]	59	1.6	0.75	29	2.0
	63	0.7/0.87	0.64	39	2.0
	53	0.87	0.57	42	2.0
Suzuki–Smith [6]	204	0.01...0.08			0.13...0.77
Van Deemter u.a. [8]	408	0.0056			0.125
		0.0225			0.333
Kawazoe u.a. [9]	97	0.067			0.51
	45	0.141			1.20

*Our evaluation of authors' data.

the constants ourselves, other values are to be found in the original literature. We also give two values useful in characterising the scale of equipment used, the column length to diameter ratio x/d_R, and the particle diameter d_P.

The axial tortuosity factor τ shows relatively little variation among the authors, and may be correlated with good accuracy by equation (40).

The radial dispersion factor β varies over a four-fold range, many authors finding rather high values. Only two publications propose a β of 10, which is close to the theoretical value of cf. 8.

The limiting Peclet number varies over a twenty-fold range, in contradiction to the usual assumption that $Pe_r = 2$ is valid. The authors who report low Pe_r, Suzuki and Smith [6], van Deemter [8], and Kawazoe [9] were experimenting with small-diameter particles, but so were Edwards and Richardson [5], who found the standard value of $Pe_r = 2$.

No correlation of results with the column length–diameter ratio x/d_R is apparent.

EXPERIMENTAL EQUIPMENT AND EVALUATION

Most of the work reported below was performed on a laboratory column made of glass, Fig. 2. The column diameter was 1.3 cm and was packed to a height of 180 cm. Sidestreams could be withdrawn for analysis at various heights; results considered below were measured at heights of 100 and 150 cm from the inlet, which was at the bottom end of the column. The column was jacketed with an outer glass tubing, and a constant temperature of 348 K was maintained by a circulatory warm water system.

Hydrogen was used as carrier gas and preheated to column temperature before passing through one port of a quick-acting valve. The second port was continuously filled with a mixture of hydrogen and methane, the tracer. At the beginning of an experiment

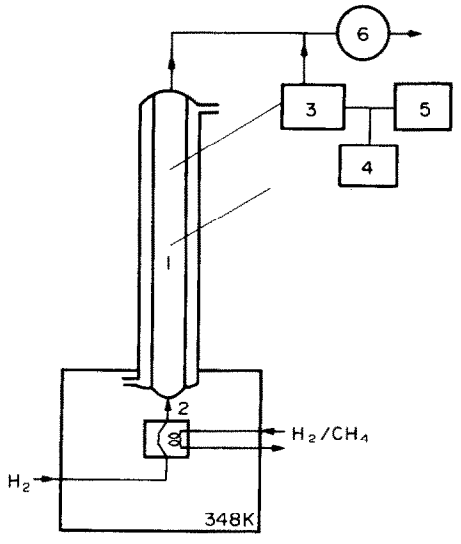

FIG. 2. Experimental equipment: 1. column; 2. sample valve; 3. detector; 4. recorder; 5. process computer; 6. gas flowmeter.

ports were exchanged and the methane flushed out of the valve and into the column. A heat-conductivity cell was employed as detector; care was taken that the sidestream connections to the detector were of equal length and diameter from all column heights. Analysis was made from only one height at a time, since withdrawal of a sidestream in this small-scale equipment was assumed to influence downstream flow conditions. The sidestream flowrate was maintained constant under all conditions, although the column flowrate was varied.

The column was packed with different charges of ballotini, glass balls of regular spheric shape. The packing diameter was varied from charge to charge.

The inlet valve was actuated by a process computer, which also recorded outlet column analysis, calculated the moments of the outlet concentration–time curve, and printed results within minutes after the experiment. We have described process-computer operation elsewhere [13].

Based on the differential equations (1)–(3) we may write

$$\mu_1' = \frac{x}{w} + \frac{t_0}{2} + t_d. \tag{45}$$

Compared to equation (4) the adsorption equilibrium constant K_1 is reduced to zero for the inert-gas measurements considered here, and the time of flushing the inlet valve t_0 does not reduce to zero at low flowrates, but averaged about 5% of μ_1'. In addition, a dead-space time t_d is involved in order to take into account the flow time between the column and the detector. This was determined in calibration runs to be 1.05 s. Since

$$w = \frac{4\dot{V}}{\varepsilon\pi d_R^2} \tag{46}$$

it is advantageous to treat the velocity of flow as a dependent variable in order to achieve high accuracy in determining D_x. We propose using equations (45, 46) for measuring the column void fraction ε, thus gaining additional information valuable for engineering purposes.

On the same basis, equation (5), reduces to

$$D_x = \frac{x^2(\mu_2 - t_0^2/12)}{2(\mu_1' - t_{0,2} - t_d)^3} \tag{47}$$

in which the possible errors in flow velocity w have been eliminated from the determination of D_x.

Preliminary data were contributed by members of our staff, H.-J. Wolff and co-workers, whom we thank for their cooperation. They were measuring moments using isobutane in air in a bench-scale column packed with zeolites. The equipment has been described previously [14]. It was possible to withdraw samples at four different heights between 48 and 228 cm from the inlet of the column, which has a diameter of 4.6 cm. The diameter of the zeolite NaMgA spheres was 0.24 cm. On the basis of the equations (4), (7) and (39) it may be

easily shown that at high flowrates

$$\frac{\left(\mu_2 - \frac{t_0^2}{12}\right)x}{2\left(\mu_1' - \frac{t_0}{2} - t_d\right)^2} = \frac{d_p}{Pe_x} + \frac{m(\beta_a + K_A)^2}{[1 + m(\beta_a + K_A)]^2} \cdot \left(\frac{R}{3k_g} + \frac{R^2}{15D_e}\right) \cdot w. \quad (48)$$

Plotting the LHS of equation (48) vs w gives a straight line permitting evaluation of Pe_x from the ordinate intercept.

DEPENDENCE OF Pe_x ON COLUMN LENGTH

The results of the preliminary measurements in the bench-scale equipment evaluated by equation (48) are shown in Fig. 3 as crosses. The decrease in Pe_x with increasing x/d_R indicates that there is an entrance zone operating close to a plug-flow mode followed downstream by a zone operating almost like an ideal mixer. This could be explained under the assumption that initially good velocity distribution is achieved by the grid supporting the packing. Since no redistributors were built into the column downstream from the entrance, the lower Pe_x may be due to increasing segregation of flow into canals and stagnant zones, particularly to enhanced flow near the wall. On the other hand the bench-scale column was operating at 200°, and was equipped with four separate electric heating segments on the outside wall which were operated at different loadings to maintain constant temperature. We therefore suspect that convective thermal currents are also responsible for a zone of high backmixing.

We have mentioned above that no particular dependence of D_x on column height is recognisable from the data in Table 1. All authors listed evaluated the difference between moments at two different heights; the x/d_R in the table are differences between values at two sampling heights. This method is recommended as a means of eliminating all entrance and sampling disturbances. The technique may be good for estimating dispersion effects in a column of semi-infinite length, but on the basis of our results does not give a true picture of what is happening in a real column. Taking the difference between moments at two heights can lead to false interpretation of results, since factors such as thermal convection are usually not included in the model equations used to describe the process. We consider it better either to measure effective dispersion effects at a given column height, or to prove that separate evaluation of moments at two different heights leads to identical dispersion coefficients. In our glass column, the open circles in Fig. 3, this holds, so that other factors than those in the model equations are negligible. Further treatment of data in this paper will be concerned only with measurements in the glass column.

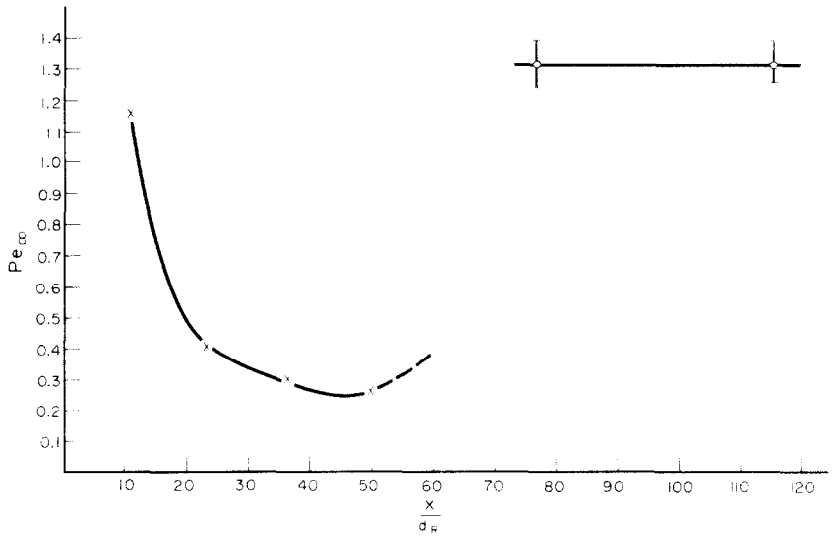

FIG. 3. Pe_x vs ratio x/d_R; ○ laboratory equipment; × bench scale equipment.

MEASURING ε FROM FIRST-MOMENT DATA

In Fig. 4 the first-moment expression $\mu_1' - (t_0/2) - t_d$ is plotted against the reciprocal linear velocity for two of the four ballotini charges at both column heights. The agreement with the straight-line equation (45) is excellent and typical of all results. The column-void fractions were determined at both heights for four particle sizes and are summarized in Table 2. Particle-void fraction was also measured in a manner standard in many laboratories. The glass balls were poured into a graduated cylinder to a volume of exactly 5 cm^3 and immersed in 5 cm^3 of water. Measuring the total mixture volume and using a simple volume balance permits a ready determination of particle void fraction, listed in column 5 of Table 2 as ε_{cyl}.

The void fractions measured by equations (45, 46),

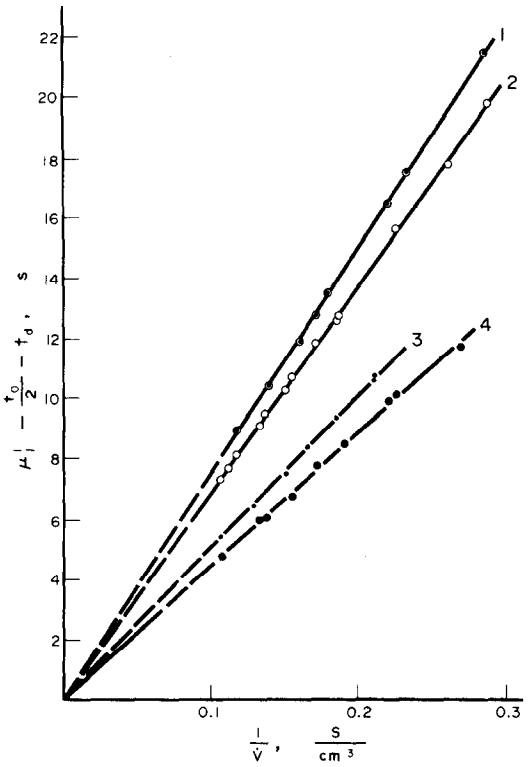

FIG. 4. First absolute moments vs reciprocal volume rate of flow at 348 K for the system methane in hydrogen: 1. x = 150 cm; d_p = 0.225 cm; 2. x = 150 cm; d_p = 0.056 cm; 3. x = 100 cm; d_p = 0.225 cm; 4. x = 100 cm; d_p = 0.056 cm.

Table 2. Void fraction of bed

1 d_p	2 x	3 ε_{col}	4 $\pm$	5 ε_{cyl}	6 $\varepsilon_{cyl}/\varepsilon_{col}$
0.056	100	0.333	0.005	0.38	1.09
	150	0.343	0.002		
0.090	100	0.364	0.004	0.39	1.07
	150	0.365	0.003		
0.139	100	0.371	0.003	0.40	1.08
	150	0.369	0.003		
0.225	100	0.377	0.003	0.42	1.11
	150	0.375	0.003		

ε_{col} are independent of column height. Noting that there was a 30 cm layer of particles above the uppermost sidestream, we conclude that a compression or expansion of particles did not occur below this point in the column. The void fraction increases with particle size according to both methods, in agreement with results of Jeschar [15] and Sonntag [16]. The void fractions measured in the cylinder are consistently larger than those in the column, which may be attributed to the differences in diameter and height of the "packed bed" in the graduated cylinder compared to the laboratory column.

The differences observed cannot be attributed to the treatment of methane as an inert gas, that is, to the assumption that $K_1 = 0$. Assuming that the cylinder values of ε are correct and calculating K_1 from equation (4) leads to negative values of the adsorption equilibrium constant, which are physically meaningless.

Thus, void fractions measured in graduated cylinders are not necessarily typical of values in packed beds even on a laboratory scale. The errors in ε would result in a 20% error in D_x, so that we advise determining the column-void fraction in the manner described above for results of high accuracy.

DETERMINING D_x FROM SECOND MOMENT DATA

The axial dispersion coefficient was calculated on the basis of equation (47) for all flowrates and particle sizes. In Fig. 5 D_x is plotted against Re and compared with curve (5) calculated using equation (39) and the constants proposed by Bischoff [3]; the agreement is poor. There is practically no difference in our results for each particle size measured at the two sidestream heights of 150 and 100 cm. Preliminary experiments had shown that for sidestreams withdrawn 50 cm from the column inlet axial dispersion coefficients did not coincide with those farther downstream.

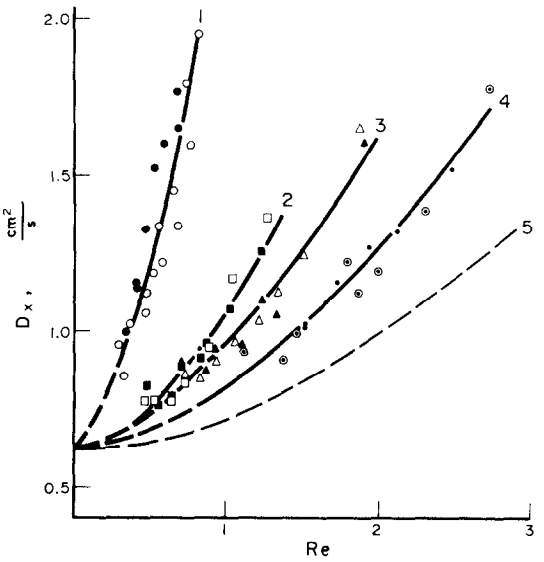

FIG. 5. Axial dispersion coefficient vs Re number for CH_4 in H_2 at 348 K. This work: 1. d_p = 0.056 cm; ○—x = 150 cm; ●—x = 100 cm; 2. d_p = 0.09 cm; □—x = 150 cm; ■—x = 100 cm; 3. d_p = 0.139 cm; △—x = 150 cm; ▲—x = 100 cm; 4. d_p = 0.225 cm; ⊙—x = 150 cm; ·—x = 100 cm; 5. calculated with constants of Bischoff [3].

In fitting equation (39) to our experimental results we calculated τ by equation (40). The value of Pe_r giving the lowest standard deviation was found for a series of β. The lowest standard deviation is shown as a function of β in Fig. 6; the corresponding Pe_r^{-1} may be found in Fig. 7. Taking the absolute minimum deviation in Fig. 6 as a criterium, the optimum $\beta - Pe_r$ combination is given for each particle diameter in Table 3. The values in the table show some scatter. However, the actual differences in deviation along each line in Fig. 6 are relatively small, and the point of absolute minimum deviation need not be significant.

There is hardly any difference in error for β varying from 10 to 30. Since previous authors (Table 1) have

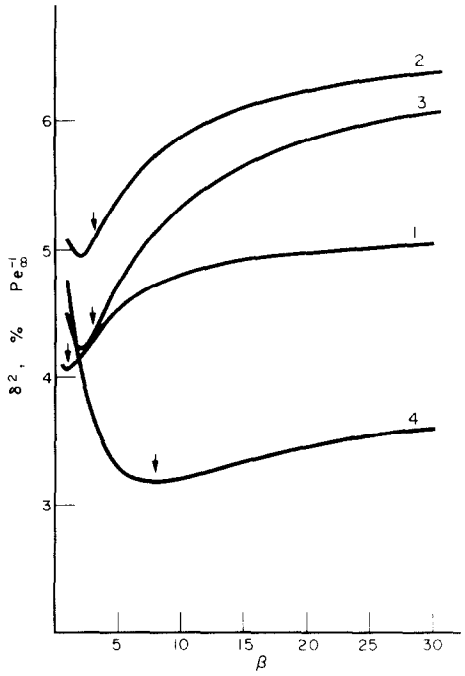

FIG. 6. Relative standard deviation from equation (39) vs radial dispersion factor β for corresponding $Pe_{z,opt.}$: 1. $d_p = 0.056$ cm; 2. $d_p = 0.09$ cm; 3. $d_p = 0.139$ cm; 4. $d_p = 0.225$ cm.

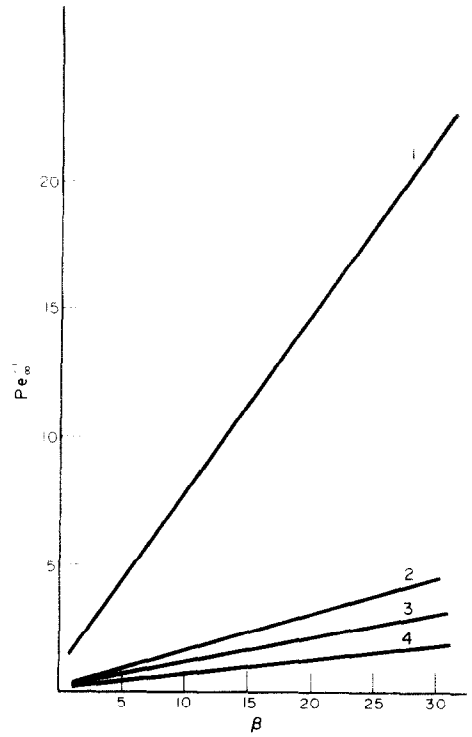

FIG. 7. Optimal Pe_z^{-1} vs β: 1. $d_p = 0.056$ cm; 2. $d_p = 0.09$ cm; 3. $d_p = 0.139$ cm; 4. $d_p = 0.225$ cm.

Table 3. Combinations of optimum parameters

d_p	β	Pe_z
0.056	1	0.57
0.09	2	1.67
0.139	2	2.04
0.225	8	1.50

chosen β in this range, we first compare our results with others treating β as a constant equal to 10.

In Fig. 8 our calculated curves (1–4) are depicted as Pe vs Re. The dashed portions of the curves lie outside of our experimental range. The shape of the curves is comparable to those in Fig. 1 found by other authors. At low Re the Pe number increases linearly with Re, in the transition range where radial dispersion is of great influence, the Pe number goes through a maximum, and approaches Pe_z at high Re. Our measurements fall within the transition region; in all cases Pe_z was determined as an extrapolated value. This was necessary, since calculations with standard methods [17] showed that the limiting Pe_z would be reached with small particles only at Re well above the point of

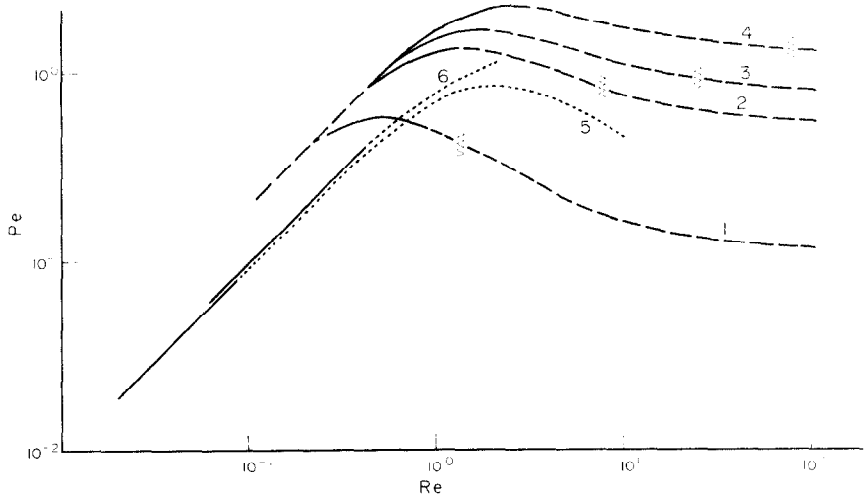

FIG. 8. Pe vs Re number. This work: CH_4 in H_2: 1. $d_p = 0.056$ cm; 2. $d_p = 0.09$ cm; 3. $d_p = 0.139$ cm; 4. $d_p = 0.225$ cm; ξ. point of incipient fluidisation. Edwards and Richardson [5]: Ar in air; 5. $d_p = 0.0377$ cm; 6. $d_p = 0.0728$ cm.

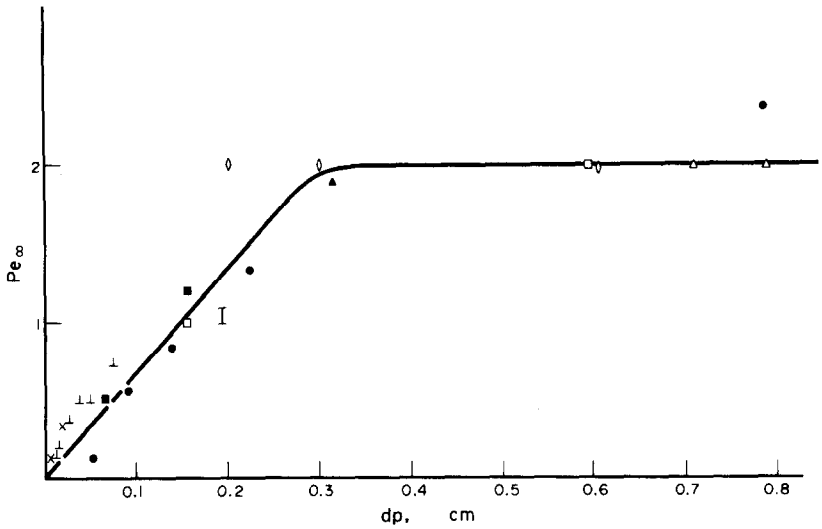

FIG. 9. Pe_∞ vs particle diameter d_p: ●—this work; ×—[8]; ■—[9]; ◇—[5]; △—[12]; ▲—[10]; □—[7]; I—[11]; ⊥—[6].

fluidisation. Our velocities were maintained at values below this point for each particle size, since the model basis for equation (39) does not apply when bed expansion becomes appreciable. If bed expansion was occurring in our column, with increasing velocity bed void fraction ε and the measured dispersion coefficient D_x should differ for the two bed heights of 100 cm and 150 cm; this is not the case. In addition, our Pe_∞ as well as those listed in Table 1 are plotted against the particle diameter in Fig. 9; the results of other authors agree with ours. There was no possibility of particle movement in the data of Suzuki and Smith [6], since their particles were trapped in a horizontal coil of 1/4 in tubing. Evans and Kenney [11] used lead balls, for which the bed expansion point is reached at Re four times larger than with our ballotini.

Further, we have considered the problem as to why Edwards and Richardson [5] did not observe low Pe_∞ with their smaller packings. Figure 8, curves 5 and 6, compares the data of Edwards and Richardson with our calculations. As above, the solid portions of curves 5 and 6 depict the experimental range whereas the dashed portions are values calculated outside of the experimental range. Their measurements were conducted entirely within the region of molecular dispersion, that is, where D_x is independent of w in equation (39), and Pe increases proportional to Re. Since they did not enter the transition range, they could not observe the deviations with smaller packings from the limiting Pe_∞ they found valid with larger packings.

The lower region of curves 5 and 6 does not coincide with the corresponding region of curves 1–4 due to differences in the Schmidt number.

INTERPRETATION OF RESULTS

The evidence in Fig. 9 supports the conclusion that a Pe_∞ of 2 applies only to packing diameters larger than 0.3 cm. For smaller particles Pe_∞ increases linearly with d_p according to the empirical equation

$$d_p \leqslant 0.25, \quad Pe_\infty = 6.7 d_p. \tag{49}$$

If $0.25 < d_p < 0.3$, there is a transition region which for technical purposes can also be approximated by equation (49). Using equation (41), γ has been calculated from Pe_∞ and $\beta = 10$ for the four particle sizes, Table 4. γ appears to be a measure of segregation of flow elements across the column diameter. Calculations of "Taylor dispersion" for laminar flow in round tubes give a value of 48. Bischoff's estimate for an average packed bed agrees with Wicke's result for an ideal packed bed. Our measurements show that γ decreases for smaller packings in accordance with the conception that channeling becomes more aggravated.

Table 4. Values of γ-factors

Source	Basis	γ
Taylor	open tube	48
Bischoff	average packed bed	22.2
Wicke	ideal packed bed	20
This paper	$d_p = 0.225$	12.9
This paper	$d_p = 0.139$	8.1
This paper	$d_p = 0.09$	5.8
This paper	$d_p = 0.056$	1.2

The same picture is obtained using the mixing-cell model, equation (43), to determine the number of particles in the axial direction comprising an average cluster. The number drops sharply with increasing particle size, Fig. 10, curve 1, and appears to be approaching Wicke's value of unity for $d_p \geqslant 0.3$. For very small sizes sixteen layers of particles lie between mixing cells; the number of mixing cells relative to the particle diameter is low, and column hydraulics are moving from the plug-flow towards the backmixer model.

Most recently Moulijn and van Swaaij [22] have come to the same conclusion. Moulijn and van Swaaij did not consider radial dispersion in their treatment; above we have held the radial dispersion coefficient constant for comparison with other authors. However,

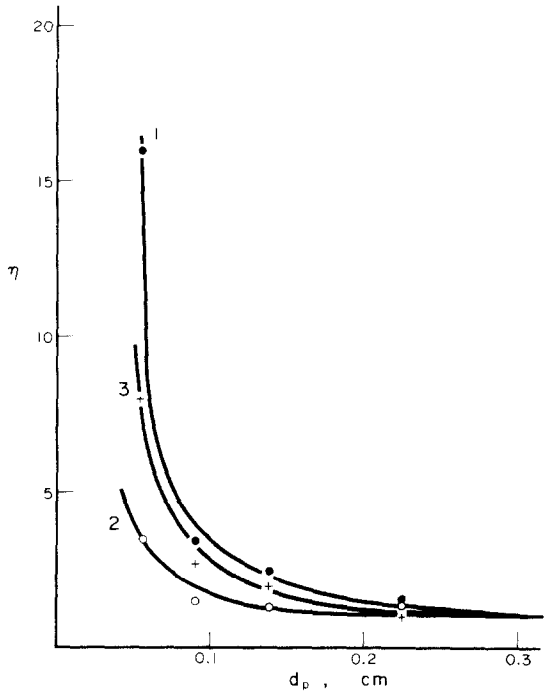

FIG. 10. Number of particles in cluster vs particle diameter. 1. n_a with $\beta = 10$; 2. n_a with near-optimum β; 3. n_r with near-optimum β.

it seems logical that if the length of clusters is growing, the width should be, too. According to equation (44), if $n_r > 1$, $\beta < 8$. The data in Table 1 show that other authors have recommended $\beta > 8$, but our data in Table 3 indicate that for smaller particles $\beta < 8$ is preferable. The particle numbers n_a and n_r are calculated from Table 3 and equations (43) and (44): smoothed lines joining the results are shown as curves 2 and 3, Fig. 10. The β-values calculated from the smoothed n_r of Fig. 10 are indicated by small arrows in Fig. 6; the corresponding Pe_r may again be taken from Fig. 7. On this basis we define curves 2 and 3 in Fig. 10 as the locus of n_a, n_r—coordinates lying close to the points of absolute minimum deviation for each individual particle size, and giving the best general description of our overall results. These values have been used to calculate the curves 1–4 in Fig. 5, in which our experimental dispersion coefficients are compared directly with the cluster model.

CONCLUSIONS

Our conclusions are analogous to those drawn in Part II for thermal dispersion. Axial mass-transfer effects are found to be larger than expected for small packing sizes and for low column length–diameter ratios. Column dispersion performance can be best explained by a model in which the number of axial particle layers as well as the number of particle diameters in the radial direction, defining the size of clusters or zones blocked to flow, increase with decreasing particle size. Correlations proposed for example by Edwards and Richardson can lead to good accuracy in technical equipment. If on the other hand catalytic reactions, adsorption breakthrough curves, ion-exchange performance etc. are being analysed in flow apparatus on a laboratory or bench scale, it is advisable to determine dispersion behavior of the particular equipment in separate runs.

REFERENCES

1. D. Gelbin, K.-H. Radecke, W. Stein and H.-J. Wolff, Stoff- und Wärmeübergang in Schüttschichten—I. Überblick und mathematische Grundlagen, *Int. J. Heat Mass Transfer* **19**, 9 (1976).
2. D. Gelbin, K.-H. Radeke, B. Rosahl and W. Stein, Stoff- und Wärmetransport in Schüttschichten—II. Wärmetransport und axiale Wärmeleitung, *Int. J. Heat Mass Transfer* **19**, 987 (1976).
3. K. B. Bischoff, A note on gas dispersion in packed beds, *Chem. Engng Sci.* **24**, 607 (1969).
4. E. Wicke, Bedeutung der molekularen Diffusion für chromatographische Verfahren, *Ber. Bunsenges.* **77**, 160 (1973).
5. M. F. Edwards and J. F. Richardson, Gas dispersion in packed beds, *Chem. Engng Sci.* **23**, 109 (1968).
6. M. Suzuki and J. M. Smith, Axial dispersion in beds of small particles, *Chem. Engng Jl* **3**, 256 (1972).
7. J. C. Urban and A. Gomezplata, Axial dispersion coefficients in packed beds at low Reynolds numbers, *Can. J. Chem. Engng* **47**, 353 (1969).
8. J. J. van Deemter, F. J. Zuiderweg and A. Klinkenberg, Longitudinal diffusion and resistance to mass transfer as causes of nonideality in chromatography, *Chem. Engng Sci.* **5**, 271 (1956).
9. K. Kawazoe, M. Suzuki and K. Chihara, Chromatographic study of diffusion in molecular-sieving, *J. Chem. Engng Japan* **7**, 151 (1974).
10. K. W. McHenry and R. H. Wilhelm, Axial mixing of binary gas mixtures flowing in a random bed of spheres, *A.I.Ch.E. Jl* **3**, 83 (1957).
11. E. V. Evans and C. N. Kenney, Gaseous dispersion in packed beds at low Reynolds numbers, *Trans. Instn Chem. Engrs* **44**, T189 (1966).
12. D. S. Scott, W. Lee and J. Papa, The measurement of transport coefficients in gas–solid heterogenous reactions, *Chem. Engng Sci.* **29**, 2155 (1974).
13. H. J. Wolff, K.-P. Roethe and D. Gelbin, Der Einsatz des Prozeßrechners TPA 1001 bei der verfahrenstechnischen Forschung, *Chem. Tech.* **27**, 209 (1975).
14. R. Weigel, Th. Fischer, B. Rosahl and D. Gelbin, Porendiffusionskoeffizienten und Tortuositätsfaktoren für Katalysatoren mittels Pulschromatographie, *Chem. Tech.* **25**, 358 (1973). *Depotbericht* **34** (1973).
15. R. Jeschar, Druckverlust in Mehrkornschüttungen aus Kugeln, *Archiv Eisenhüttenwes.* **35**, 91 (1964).
16. G. Sonntag, Einfluß des Lückenvolumens auf den Druckverlust in gasdurchströmten Füllkörpersäulen, *Chemie-Ingr-Tech.* **32**, 317 (1960).
17. J. Beranek, G. Winterstein and K. Ross, *Grundlagen der Wirbelschichttechnik*. VEB Deutscher Verlag für Grundstoffindustrie, Leipzig (1975).
18. D. J. Gunn and C. Pryce, Dispersion in packed beds, *Trans. Instn Chem. Engrs* **47**, T341 (1969).
19. F. DeMaria and R. R. White, Axial dispersion in packed beds, *A.I.Ch.E. Jl* **6**, 473 (1960).
20. R. J. Sinclair and O. E. Potter, The dispersion of gas in flow through a bed of packed solids, *Trans. Instn Chem. Engrs* **43**, T3 (1965).
21. J. J. Carberry and R. H. Bretton, Axial dispersion of mass in flow through fixed beds, *A.I.Ch.E. Jl* **4**, 367 (1958).
22. J. A. Moulijn and W. P. M. van Swaaij, The correlation of axial dispersion data for beds of small particles, *Chem. Engng Sci.* **31**, 845 (1976).

TRANSFERT DE CHALEUR ET DE MASSE DANS LES LITS FIXES—III. DISPERSION MASSIQUE AXIALE

Résumé—Les techniques chromatographiques et la méthode des moments statistiques sont utilisées pour déterminer les coefficients de dispersion axiale du méthane dans l'hydrogène sur des billes de verre, de différents diamètres, disposées dans une petite colonne. Quelques résultats supplémentaires sur la dispersion axiale de l'isobutane dans l'air pour une colonne pilote avec soutirage d'échantillon à différentes hauteurs. Les effets de dispersion sont difficiles à estimer pour les faibles rapports longueur de colonne-diamètre. Les coefficients de dispersion sont plus grands avec des garnissages petits; la valeur limite de P^{∞} aux grands débits croît linéairement avec le diamètre du garnissage pour $d^p \leqslant 0{,}25$ cm et n'atteint la valeur généralement admise $P^{\infty} = 2$ que lorsque $d^p \geqslant 0{,}3$ cm. Ces résultats sont expliqués à partir d'un modèle dans lequel le nombre de cellules de mélange en série décroît avec le diamètre de particule à cause de l'accroissement du nombre de particules agglomérées. Les formules connues pour les coefficients de dispersion axiale peuvent conduirent à une bonne précision dans les réalisations techniques, mais l'analyse des opérations en laboratoire ou à l'échelle pilote nécessite une recherche particulière.

WÄRME- UND STOFFÜBERTRAGUNG IN SCHÜTTSCHICHTEN —III. AXIALE MASSENDISPERSION

Zusammenfassung—Mit Hilfe der Chromatografie und der statistischen Momentenmethode werden Axialdispersionskoeffizienten für Methan in Wasserstoff auf Glaskugeln unterschiedlichen Durchmessers in einer Laborsäule untersucht. Einige zusätzliche Daten sind für die Axialdispersion von Isobutan in Luft in einer Versuchssäule mit Probenentnahme in verschiedenen Höhen vorhanden. Dispersionseffekte können beim Verhältnis geringer Säulenlänge zum Durchmesser unvorhersagbar sein. Dispersionskoeffizienten sind bei kleineren Füllkörpern größer. Der Grenzwert von Pe_{∞} bei hohen Stoffströmen erhöht sich für $d_p \leqslant 0{,}25$ cm linear mit dem Durchmesser der Füllkörper und erreicht erst für $d_p \geqslant 0{,}3$ cm den im allgemeinen angenommenen Wert $Pe_{\infty} = 2$. Diese Ergebnisse werden durch ein Modell erklärt, bei welchem die Zahl der hintereinanderliegenden Mischzellen mit dem Partikeldurchmesser abnimmt, da bei einer zunehmenden Zahl von Teilchen Klusterbildung auftritt. In der Literatur angegebene Korrelationen zur Vorhersage von Axialdispersionskoeffizienten können bei technischen Anglagen zu guter Genauigkeitführen, die Analyse von Prozessen in Schüttschichten im Versuchs- oder Labormaßstab sollte aber eigene Untersuchungen des Dispersionsverhaltens einschließen.

ТЕПЛО- И МАССОПЕРЕНОС В ПЛОТНЫХ ПСЕВДООЖИЖЕННЫХ СЛОЯХ. III. АКСИАЛЬНОЕ ДИСПЕРГИРОВАНИЕ МАССЫ

Аннотация — С помощью хроматографической техники измерений и метода статистических моментов определены коэффициенты аксиальной дисперсии метана в водороде на стеклянных шариках различных диаметров, помещенных в лабораторную колонну. Представлены дополнительные сведения об аксиальной дисперсии изобутана в воздухе в стендовой колонне, полученные путем отбора проб на различных высотах. При небольших отношениях длины колонны к её диаметру дисперсия учету не поддается. Коэффициенты дисперсии тем выше, чем меньше диаметр частиц в слое. Предельное значение критерия Pe_{∞} при больших массовых расходах увеличивается линейно с увеличением диаметра упаковки, если $d_p \leq 0{,}25$ см, и только при $d_p \geq 0{,}3$ см достигает общепринятого значения $Pe_{\infty} = 2$. Полученные результаты поясняются на модели, в которой число последовательно соединенных ячеек смешения уменьшается с уменьшением диаметра частиц из-за их коагуляции. Приводимые в литературе обобщенные соотношения для расчета коэффициентов аксиальной дисперсии являются достаточно точными для расчета промышленных установок, однако требуют уточнения при анализе процессов в плотном слое, происходящих в лабораторных или стендовых установках.